Experimental investigation of a confined flat two-phase thermosyphon for electronics cooling

Marine Narcy, Stéphane Lips, Valérie Sartre

EXPERIMENTAL INVESTIGATION OF A CONFINED FLAT TWO-PHASE THERMOSYPHON FOR ELECTRONICS COOLING

Marine Narcy*, Stéphane Lips, Valérie Sartre
Univ Lyon, CNRS, INSA-Lyon, CETHIL UMR5008, F-69621, Villeurbanne, France
*marine.narcy@insa-lyon.fr

A novel type of two-phase heat spreader based on a flat confined thermosyphon is proposed for electronics cooling applications. Two wickless flat copper-water heat pipes with an inner thickness of 3 mm were experimentally investigated for both two-phase flow visualizations and characterization of thermal performance. The effects of heat input, filling ratio, inclination and saturation temperature were studied. Experimental results show that the confinement of the fluid inside the heat spreader induces confined boiling phenomenon with a strong coupling between condensation and boiling mechanisms. They also highlight an enhancement of heat transfer and interesting performance such as high heat transfer capability (tested up to 30 W/cm² with a corresponding thermal resistance around 0.07 K/W at an optimum filling ratio), low sensitivity to inclination and higher degree of freedom on heat sources location compared to a classical thermosyphon.

Keywords: heat pipe, two-phase heat spreader, thermosyphon, confined boiling

1. INTRODUCTION

Due to perpetual advances in electronic engineering with the pursuing of higher performance and device miniaturization, thermal management of electronic components requires to deal with continuously increasing heat fluxes and local temperatures: between the years 2000 and 2010, the associated heat fluxes have multiplied by more than ten, eventually reaching 120 – 150 W/cm² for some applications (Faghri, 2014). Since the lifetime and reliability of electronic components is sensitive to their operating temperature, these increasing demands on heat dissipation create a need for efficient devices with high heat transfer and heat spreading capabilities.

Heat pipes (Reay *et al*, 2013) and micro heat pipes (Sobhan *et al*, 2007) were first considered as an adequate solution for electronics cooling with their high effective thermal conductivity, passiveness, and performance for temperature control. However, today's requirements highlight their limitations in terms of heat transfer and temperature uniformity (Faghri, 2014). Two-phase thermosyphons, also known as wickless or gravity-assisted heat pipes, therefore emerged as an alternative for small-scale applications with better thermal performance (Jafari *et al*, 2016).

The main physical mechanisms taking place in a classical two-phase closed thermosyphon (TPCT) are illustrated in Figure 1. A heat flux is supplied to the working fluid through the evaporator wall in the lower section of the device, causing the liquid contained in the cavity to start to evaporate. Vapor flows upwards in the pipe up to the condenser region where it condenses on the inner wall, forming a liquid film that is returned back to the evaporator by gravity.

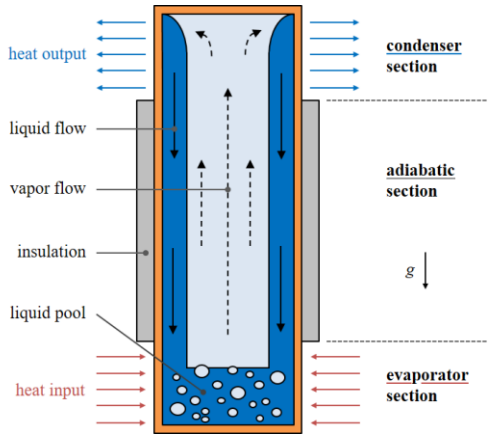

Figure 1. Operating principle of a thermosyphon.

Because of the significant latent heat of vaporization associated to phase change, a large amount of heat can be transferred from the evaporator section to the condenser section with a very small relative temperature difference. If the condensation area is larger than the evaporation area, the device also acts as a heat spreader.

TPCTs generally do not include wick structures, unlike conventional heat pipes: since gravity is the major driving force for condensate return, they do not exhibit a large flow resistance or low boiling limit inside the wick, which is of great interest for high heat flux applications where conventional heat pipes show limitations.

In addition to their high heat transfer and spreading capability, TPCTs have other interesting features for electronics cooling in challenging environments such as aeronautical environments: their geometry can easily be adapted to fit power modules or flat electronic components, or to meet space constraints; with the absence of wick, they are also simpler and cheaper to manufacture and do not raise the issue of frozen start-up in capillary structure.

However, TPCTs are constrained by other operating parameters since their thermohydraulic behavior is strongly affected by the heat input, the filling ratio, the working fluid and the device design.

In particular, TPCTs are very constrained regarding the heat source location: the evaporator section has to be at the same level than the liquid pool to avoid dry-outs of the liquid film, which requires a vertical positioning of the heat source below the condenser section, at the very bottom of the device (Jafari *et al*, 2016). TPCTs are also characterized by a high sensitivity to inclination since gravity ensures the condensate return to the evaporator. The influence of the inclination angle on the thermal performance of classical thermosyphons was studied by various authors (Noie *et al*, 2007; Ong *et al*, 2014; Zhang *et al*, 2014, Hu *et al*, 2016…) with different quantitative conclusions depending on the working fluid and heat pipe geometry. Nevertheless, consistent trends were observed with significant changes in the thermal resistance according to inclination angle and optimum conditions in intermediate configurations between vertical and horizontal positions, which can be a problem in the case of applications where the inclination is expected to change.

These drawbacks may nonetheless be limited by introducing an additional geometrical parameter, the confinement of the fluid inside the heat pipe. Indeed, the inner diameter (for cylindrical or annular thermosyphons) or the inner thickness (for flat thermosyphons) plays an important role in the balance of forces that rule boiling phenomena in the device. Decreasing this dimension to small scales promotes surface tension forces over buoyancy forces, which could limit the influence of the inclination angle through gravity forces, for instance.

The condition for a TPCT to be considered confined can be related to a low Bond number *Bo* indicating that the forces due to surface tension are not negligible (Terdtoon *et al*, 1999; Franco and Filippeshi, 2013) or to characteristic length comparable to expected bubble departure diameter (Jouhara and Robinson, 2010) or capillary length of the working fluid.

Moreover, confined boiling phenomena are often associated with an enhancement of heat transfer in pool boiling. Bonjour and Lallemand (1998) experimentally studied boiling in a confined rectangular vertical channel and provided flow patterns maps based on *Bo* number including flow regimes corresponding to heat transfer enhancement. Similar conclusions were reached in cylindrical confined spaces by Rops *et al* (2009). They showed that the heat transfer enhancement for nucleate boiling regimes is induced by an increase in the vapor velocity and the liquid entrainment rate through the confinement of the channel that “squeezes” the vapor bubbles.

A confined TPCT may therefore exhibit better thermal performance with reduced limitations.

The present study aims at proposing a novel type of two-phase heat spreader for electronics cooling in constrained configurations such as in aeronautical environments, by combining features of two-phase thermosyphons and confined two-phase systems. Considering the requirements in terms of thermal management of electronic components, and the advantages and drawbacks of TPCTs, a suitable heat spreader would consist in a flat confined two-phase thermosyphon.

However, classical thermosyphons used in solar or deicing systems need to be adapted to this type of application with limited available space; the consequent changes in both dimensions and geometry (especially the changing from cylindrical to flat geometry) are going to significantly affect the two-phase flow and thermal performance of the spreader (Jafari *et al*, 2016). The introduction of the confinement is also expected to induce major changes in the flow patterns and thermal resistance due to the strong coupling between boiling and condensation processes (Zhang *et al*, 2013).

Thus, an extensive experimental investigation of this new heat spreader is necessary to understand the underlying thermohydraulic phenomena and propose adequate designs to meet challenging specifications such as high heat fluxes, compactness, changing inclination or large degree of freedom on the heat source location. In particular, visualizations of flow patterns are needed to characterize the complicated two-phase behavior and correlate it with thermal performance. Experiments with direct visualizations are complex and then rarely performed. Some observations were realized in relatively large transparent cylindrical TPCTs by Li *et al* (2016), Smith *et al* (2016) or using electrical capacitance tomography (Liu *et al*, 2007). Existing results from flow visualizations are often partial and the conditions in which they were obtained are most of the time not clearly indicated. A proper characterization of the heat spreader therefore requires an appreciation of the influence of various operating parameters in addition to flow patterns description.

In order to achieve this goal, a flat confined TPCT with adapting front panel was designed and built, as detailed in Section 2. This heat spreader relies on confined boiling phenomena to ensure proper operation in various constrained configurations and provided flow visualizations and assessments of thermal performance that are discussed in Section 3.

2. EXPERIMENTAL SET-UP AND DATA REDUCTION

2.1. Experimental set-up

The experimental set-up built to study the heat spreader is presented in Figure 2. The device is connected to the graduated filling system and mounted on an inclinable support that allows to choose an inclination angle θ between 0° and 180° (horizontal position with evaporator and condenser on top, and horizontal position with evaporator and condenser on the bottom, respectively, with θ = 90° corresponding to the vertical configuration of the schematics).

Two different configurations were investigated, as presented in Figure 2a and Figure 2b, respectively, with variations in the heat sink and heat source dimensions and / or location; they are thereafter referred to as Config 1 and Config 2.

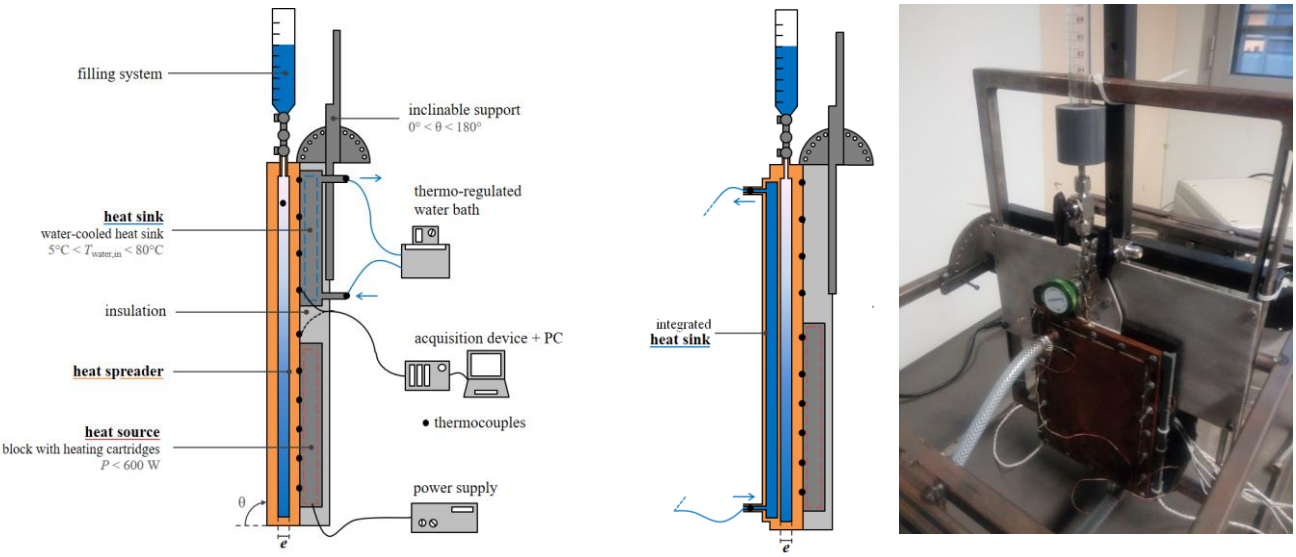

(*a*) Configuration 1 - separated back heat sink cross-section schematics

(*b*) Configuration 2 – integrated front heat sink cross-section schematics and front picture with the copper heat spreader

Figure 2. Experimental set-up, zoom on the test bench with the heat spreader.

The temperature and flow rate of the water-cooled heat sink are controlled by a thermo-regulated bath, with cooling water inlet temperature $T_{cool,in}$ between 5 °C and 80 °C. Two different versions of the heat sink were tested: a 10 cm × 8 cm separated heat sink on the top section of the back wall [Config 1], as shown in Figure 2a, and a 12 cm × 18 cm heat sink integrated in the whole front panel [Config 2], as illustrated in Figure 2b.

Two different heat sources made of an aluminum block with three heating cartridges powered by a power supply delivering up to 600 W were used: a 10 cm × 6 cm heat source simulating a power module for an existing application [Config 1] and an 8 cm × 2.5 cm heat source to investigate higher heat fluxes [Config 2]. The chosen heat source is insulated and installed on the lower half of the back wall of the heat spreader. Heat fluxes up to 30 W/cm² were supplied.

Electrical heating power measured with the current and voltage, and temperatures from the spreader and the heat sink are recorded by a Keithley data acquisition system and monitored on a LabVIEW interface.

In all configurations, the parameters that can be set by the experimenter are the filling ratio *FR* (given as a percentage of the spreader volume), the cooling water inlet temperature $T_{cool,in}$ (heat sink), the heating power *Q* (heat source) and the inclination angle of the device θ. Corresponding ranges of settings are summarized in Table 1.

Table 1. Experimental ranges for operating parameters.

Set parameters	**Notation**	**Experimental range**
Filling ratio	*FR*	0 – 100 %
Heating power	*Q*	0 – 600 W
Water cooling inlet temperature	$T_{cool,in}$	5 °C – 80 °C
Inclination angle	θ	0° – 180°

The heat spreader itself consists in a copper sealed flat container where vacuum is made and that is then filled with a variable amount of water, in the same way as a thermosyphon. Water was chosen as the working fluid because of its compliance with aeronautical specifications, its performance for the targeted application and its compatibility with copper.

The back panel of the heat spreader is a 3mm thick copper plate of dimensions 12 cm × 18 cm with inner vertical superficial 200 µm wide grooves that are used for heat transfer enhancement and not as a capillary structure. The front panel is 2.5 mm thick and declined in two versions for the device to adapt to two different functions: it is either in copper (and includes the water-cooled heat sink, for a full copper spreader, as in Figure 3b) to easily characterize thermal performance during parametric runs or in polycarbonate (transparent spreader, as in Figure 3a) to provide flow visualizations. In both cases, the thickness of the inner cavity (denoted *e* in Figure 2) is 3 mm, i.e. close to the capillary length of water, which ensures the system confinement and induces confined boiling phenomena.

The sealing of the heat spreader is made using an O-ring and screws; spacers are added to brace the two panels. Finally, every surface that is not used for flow visualization is insulated with foam to limit heat losses.

(*a*) transparent heat spreader
[copper base, polycarbonate panel, Config 1]

(*b*) copper heat spreader
[copper base, copper panel, Config 2]

Figure 3. Pictures of the heat spreader.

In a given configuration, both versions of the spreader use the same copper base with the same heat sink and heat source. A common set of 10 K-type thermocouples with a precision of ± 0.1 °C measures the outer wall temperature on the heated side, allowing to obtain a temperature distribution on the entire height of the heat spreader, as illustrated in the schematics of Figure 2. In Config 1, the distance between the evaporator and condenser sections is too short to enable the presence of an actual adiabatic section; two wall-crossing K-type thermocouples are therefore added to each front panel to measure the temperature inside the cavity, relatively far from the liquid film, in the upper section of the spreader (as indicated by two black dots in Figure 3a) and thus provide an estimation of the saturation temperature T_{sat}.

2.2. Data reduction

The temperature difference along the heat spreader $\Delta T_{spreader}$ can be considered as a preliminary indication of its thermal performance. It is written according to the outer wall temperatures at the evaporator and at the condenser, with the notations presented in Figure 4:

$$\Delta T_{\text{spreader}} = T_{\text{w,max}} - T_{\text{w,min}} \quad (1)$$

The thermal resistance of the heat spreader $R_{spreader}$, that is primarily used to characterize its thermal performance, is expressed with this temperature difference and the heat load Q supplied in the evaporator section:

$$R_{\text{spreader}} = \frac{\Delta T_{\text{spreader}}}{Q} \quad (2)$$

According to Figures 2a and 4, in Config 1, the temperature at the condenser $T_{w,min}$ is known and the spreader thermal resistance $R_{spreader}$ is directly measured. However, in Config 2, the temperature distribution on the back side does not allow to get the temperature at the condenser $T_{w,min}$ and a global thermal resistance R_{th} including both the spreader and the heat sink is measured between $T_{w,max}$ and $T_{cool,in}$. The thermal resistance of the heat sink $R_{heat\ sink}$ is then estimated with correlations of the literature according to operating parameters and $R_{spreader}$ is obtained by subtraction:

$$R_{\text{spreader}} = R_{\text{th}} - R_{\text{heat sink}} \quad (3)$$

Analysis of temperature profiles provides additional information about the spreader thermal performance, such as maximal rewetted height and preferential areas for heat source location, which can be compared to more precise values processed from flow visualizations.

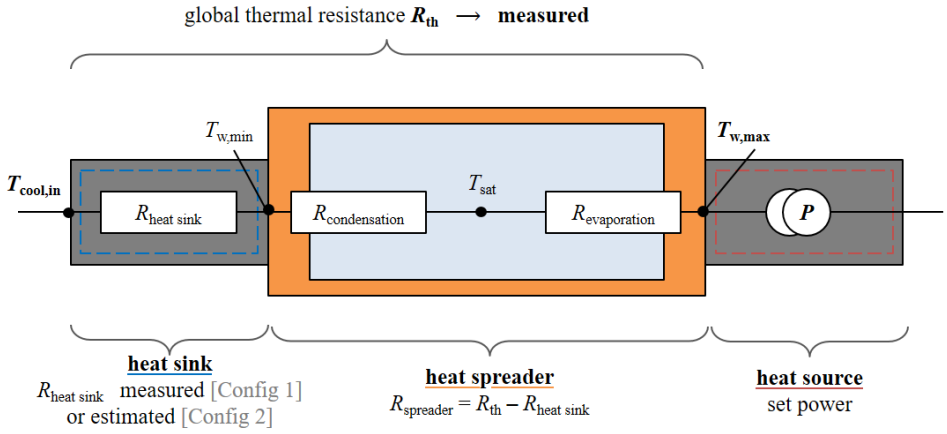

Figure 4. Illustration of thermal resistances for data processing.

Uncertainties need to be properly determined to draw relevant quantitative conclusions on the influence of operating parameters on the spreader thermal performance.

In the case of Config 1, the uncertainty in the spreader thermal resistance depends on the uncertainties in the wall temperatures and applied heat flux. Since the temperature distributions on the evaporator and condenser sections are relatively uniform, the wall temperatures $T_{w,max}$ and $T_{w,min}$ are obtained by averaging the temperature measurements along these sections. The estimation of the uncertainty in the heat load is more complex. An energy balance is performed to quantify heat losses: the input power at the evaporator section $Q = Q_{in}$ (obtained using the supply voltage and current measurements) is compared to the heat load removed at the condenser Q_{out}:

$$Q_{out} = \dot{m} \cdot Cp \left(T_{cool,out} - T_{cool,in}\right) \quad (4)$$

The corresponding experimental uncertainty in Q was found to be around 15% for low power settings and 7% for high power settings, which is consistent with the usual order of magnitude for heat losses in this type of configuration.

The resulting uncertainty in the spreader thermal resistance $\delta R_{spreader}$ was then calculated with the expression:

$$\frac{\delta R_{spreader}}{R_{spreader}} = \sqrt{\left(\frac{\delta Q}{Q}\right)^2 + \left(\frac{\delta \Delta T_{spreader}}{\Delta T_{spreader}}\right)^2} \quad (5)$$

which yields an uncertainty in $R_{spreader}$ between 8% and 16%, depending on the supplied heat load.

Measurement uncertainties in other operating parameters can be mentioned, but their effect on the estimation of the thermal performance is hardly quantifiable. It is the case, for instance, for the filling ratio (measured with a precision of ± 1 mL, corresponding to an uncertainty between 3% and 20%) or inclination angle.

3. RESULTS AND DISCUSSION

This section presents and discusses the experimental results obtained with the different heat spreaders. Flow regime visualizations are used to understand the working principle of a flat confined thermosyphon and to highlight the high coupling between boiling and condensation processes while the influence of various parameters on the thermal resistance is assessed to characterize its thermal performance.

3.1. Flow visualizations and operating principle

The confinement of the working fluid inside the two-phase thermosyphon is ensured by choosing an inner thickness e close to the capillary length of the working fluid l_{cap}, which is validated by the calculation of the Bond number Bo that allows to compare the effects of gravitational forces and capillary forces and can be expressed according to these two characteristic lengths:

$$Bo = \frac{\left(\rho_{liq} - \rho_{vap}\right) g\, e^2}{\sigma} = \frac{e^2}{{l_{cap}}^2} \quad (6)$$

For water, the capillary length l_{cap} is equal to 2.7 mm. With a 3 mm inner thickness, a Bond number of 1.2 is achieved, which confirms that the surface tension forces are not negligible as in unconfined systems without capillary structure, and that the confinement induces a new force balance with changes in flow patterns and thermal performance.

Visualizations of flow regimes are therefore necessary to understand the underlying boiling mechanisms and correlate thermal performance with thermohydraulic phenomena. Due to experimental obstacles and specificity of each device and configuration, they are however difficult to obtain, and complete flow pattern maps are rarely provided. In the present

study, series of tests with the transparent heat spreader were conducted to gather information on flow regimes and effects of confined boiling, as illustrated in Figure 5, for various heating and cooling conditions.

Two main flow patterns were observed depending on heating conditions.

For low saturation temperatures, large and scarce bubbles (as delimited in Figure 5b) nucleate in the evaporation area and rise to the top of the device where they are condensed. The frequency of bubble appearance in this regime increases with the heat flux. For the higher values of heat input, the large amounts of liquid that are periodically vaporized and rapidly propelled to the condenser section seem to prefigure geyser boiling as described by Tong *et al*. (2015).

At high saturation temperature, very numerous and small bubbles nucleate in the evaporation area, with a high appearance frequency. As they rise to the condenser section, some of these bubbles are deviated to the sides of the device by the condensate returning to the evaporator, creating a "bubble tree" as observed in Figure 5c. Depending on the test conditions, large coalesced bubbles can also be observed above this tree.

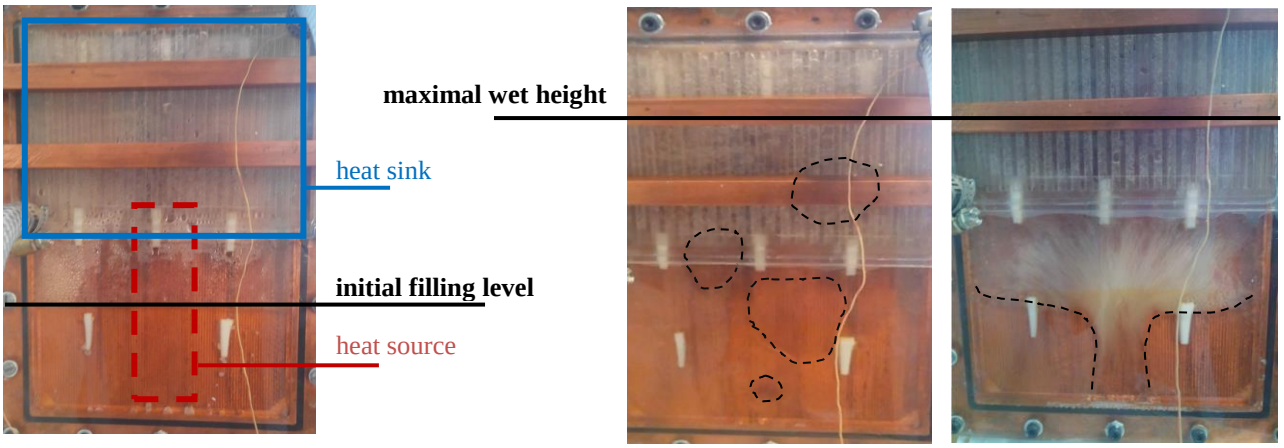

(*a*) without heating

(*b*) low saturation temperature (typically T_{sat} < 60 °C)

(*c*) high saturation temperature (typically T_{sat} > 60 °C)

Figure 5. Flow visualizations with the transparent heat spreader.
initial filling ratio: 30% of the spreader volume, Q = 500 W in (*b*) and (*c*)

The two flow regimes differ by the frequency and size of nucleated bubbles (periodic detachment of large bubbles at low saturation temperature, and continuous nucleation of small bubbles at high saturation temperature) but both flow patterns lead to an increase in the rewetted height, as illustrated in Figure 5 with the difference between the initial liquid level (corresponding to a filling ratio of 30 % of the spreader volume) and the maximal wet height. This rewetting ensures that there is no dry-out of the liquid film and no wall overheating, even in the portion of the evaporator section that is not immerged in the liquid pool. It can be explained by considering the operating principle of the confined flat thermosyphon that is illustrated in the schematics (front view and cross-section) of Figure 6.

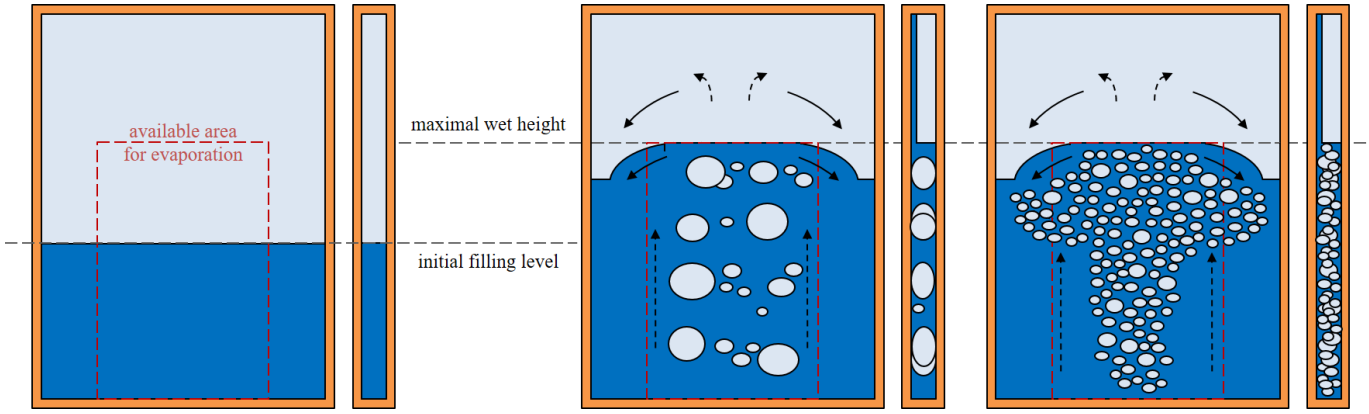

(*a*) without heating

(*b*) low saturation temperature

(*c*) high saturation temperature

Figure 6. Heat spreader operating principle.

The operating principle of the two-phase heat spreader is described in a patent that was filed for the particular device that is studied here (Lips *et al*, 2017). In the confined space, the interaction between gravitational, buoyancy and capillary forces induces a liquid flow that rewets a large area of the inner wall which is not in contact with the liquid before operation. Indeed, in the case of low saturation temperatures, large bubbles nucleating in the evaporation area or coalescing in the liquid pool are confined and tend to "push" the liquid above upwards as they ascend to the condenser section. In the case of higher saturation temperatures, the significant amount of vapor produced by dense fully developed nucleation also contributes to an increase of the rewetted height. The liquid returns to the evaporator section under the form of a film, mostly in the side sections.

The rewetted surface depends on the initial filling level and volume of nucleated bubbles: in the case of low filling ratios with moderate heat fluxes, the rewetted height is not very significant. Optimum rewetting is achieved with relatively consequent filling ratios (typically between 25 % and 80 % of the spreader volume, depending on the configuration and according to flow visualizations) and boiling regimes with dense fully developed nucleation. In these configurations, the rewetted height can reach twice the length corresponding to the initial filling level. As long as one heat source is kept under the liquid pool level, heat sources can be added on the whole rewetted height, therefore extending the available evaporation area and allowing the heat spreader not to be as constrained as classical thermosyphons in regards with the heat source location.

3.2. Heat spreader performance

As previously mentioned, the heat spreader thermal resistance is affected by numerous operating parameters. In the present work, the influence of the heating power, filling ratio, inclination angle and saturation temperature is investigated with the copper heat spreader to assess the performance of the novel confined flat TPCT. Unless indicated otherwise, results presented here correspond to Configuration 1 with the heat sink on the same side than the heat source.

Influence of heating power

Figure 7 presents examples of temperature distributions with steady state temperatures at different locations on the outer back wall for various filling ratios *FR* and various heating powers *Q*. Measurements corresponding to thermocouples in the middle region of the evaporator section and condenser section are relatively, which justifies the averaging of these values to obtain the respective temperatures $T_{w,max}$ and $T_{w,min}$. The short distance between the heat source and the heat sink does not allow to get a proper estimation of the saturation temperature, as can be seen from the graphics, hence the use of additional thermocouples in the cavity.

The temperature difference between the evaporator and condenser sections is representative of the spreader thermal performance. At fixed filling ratio and inlet cooling temperature, it increases with the supplied heat load until dry-out of the liquid film. For $T_{cool,in}$ = 40 °C, all filling ratios considered, a maximal temperature difference $\Delta T_{spreader}$ of 45 K was measured between the evaporator and condenser for a 30 W/cm² heat flux.

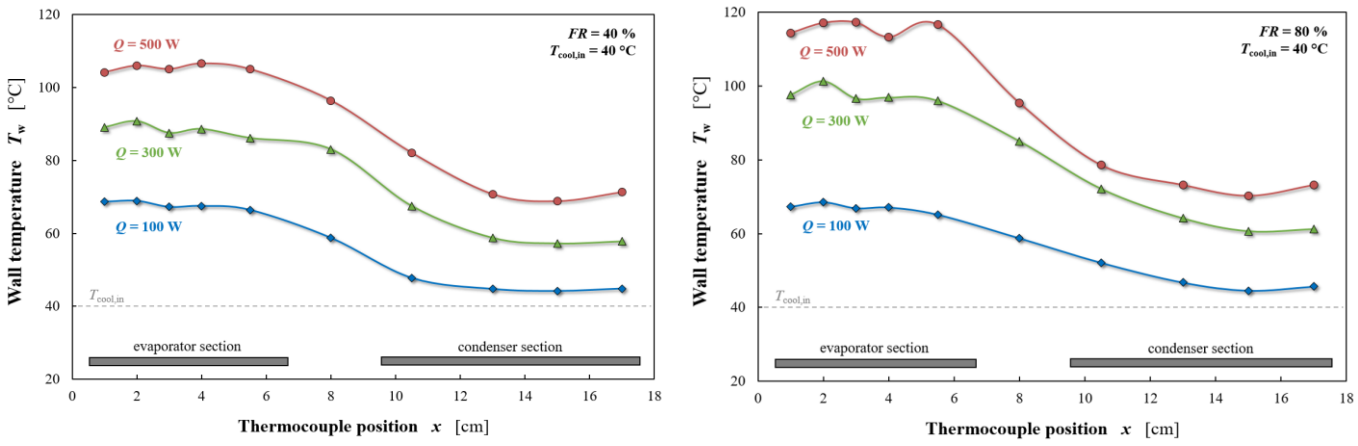

(*a*) *FR* = 40 % (*b*) *FR* = 80 %

Figure 7. Outer wall temperature distribution for various filling ratios and input powers - $T_{cool,in}$ = 40 °C.

Figure 8 presents an example of evolution of the spreader thermal resistance according to the heating power up to 30 W/cm² (600 W) for four filling ratios, at constant inlet cooling temperature $T_{cool,in}$ = 40 °C. The thermal behavior of the system is non-linear with low heat resistance for high heat fluxes and a slight degradation of thermal performance for lower heat fluxes. Low supplied heat load (Q < 100 W) mostly correspond to heating conditions that do not allow boiling to start. Thermal resistances down to 0.07 K/W were reached for the maximal tested heat flux around 30 W/cm², as can be seen for the curve corresponding to the 40 % filling ratio.

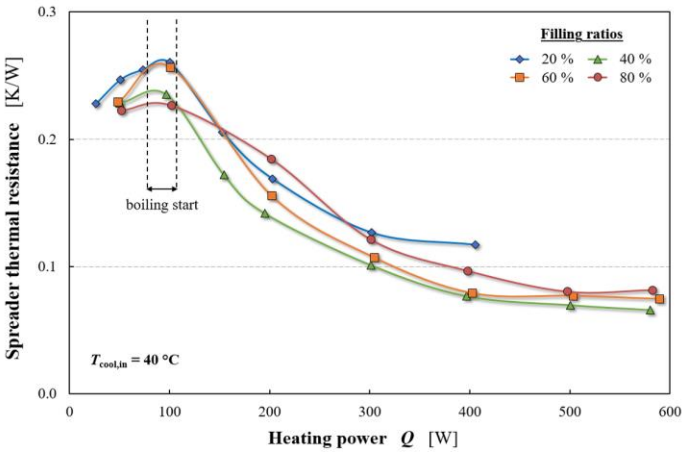

Figure 8. Evolution of the spreader thermal resistance with the heating power for various filling ratios.

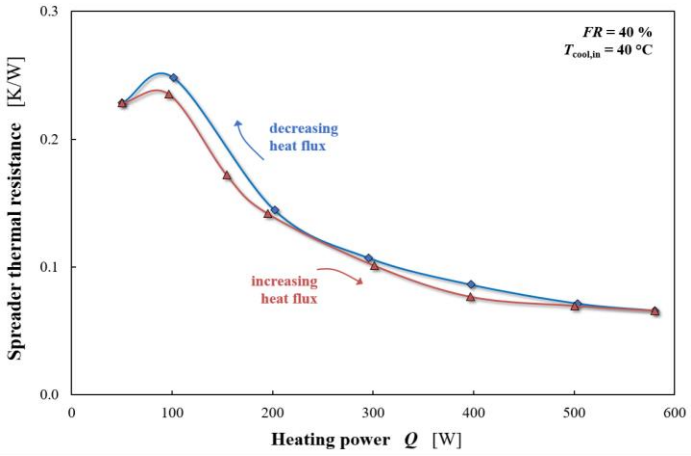

Figure 9. Hysteresis effect for *FR* = 40 %.

Operation with very low temperature differences may however exhibit hysteresis behavior, with nucleate boiling being sustained down to temperature differences below the level needed to initiate boiling. Experiments were therefore performed to draw hysteretic loops, as the one in Figure 9, by characterizing the thermal resistance first with increasing heat fluxes and then with decreasing heat fluxes. Hysteresis effect depends on the filling ratio, but it is rather limited on the present temperature ranges (the maximal difference between the two curves corresponds to the experiments with the 40 % filling ratio that are presented here and is not significant compared to the uncertainty in the thermal resistance). This conclusion was already reached by Ong *et al.* (1997) for vertical TPCT using water.

The thermal resistance measurements provided by the flat confined thermosyphon can be compared to literature values obtained with flat confined heat pipes or two-phase thermosyphons in comparable operating conditions. For instance, Li and Lv (2016) listed experimental studies including investigation of thermal resistance of flat plate heat pipes that can be considered confined. Experiments that were performed with copper-water devices on similar ranges of heat flux and cooling temperature exhibit thermal resistances between 0.2 K/W and 0.9 K/W, which is 3 to 14 times worse than what the present heat spreader delivered in optimum configuration. These values highlight an enhancement of thermal performance compared to flat plate heat pipes that are still limited in terms of heat transfer capability.

Experimental results are in better agreement with the values of thermal resistance obtained by Jouhara and Robinson (2010) in a small diameter TPCT filled with water and presenting very similar dimensions: the authors validated the confinement of their device by comparing its inner diameter to the expected bubble departure diameter and measured overall thermal resistances down to 0.14 K/W for a 260 W supplied heat load and cooling temperature of 35 °C. The consistency of the two studies is interesting, considering that only the geometry significantly varies.

Influence of filling ratio

As observed by comparing Figures 7a and 7b, the spreader thermal performance is strongly affected by the filling ratio. Parametric runs were therefore conducted for various filling ratios between 20 % and 80 % of the spreader volume.

Figure 8 shows that, in the studied regimes, the thermal resistance increases with the filling ratio, with the exception of a thermal performance degradation at very low filling ratio as illustrated with the curve for *FR* = 20 % that exhibits a liquid level too low to correctly rewet the whole evaporator section. An optimum filling ratio could therefore be determined for each set of cooling and heating conditions. In the case illustrated in Figure 8, this optimum filling ratio appears to be between 20 % and 40 % of the spreader volume, i.e. between 50 % and 100 % of the evaporator volume. Zhang *et al.* (2013) also found out that an optimum filling ratio allows an enhancement of heat transfers by promoting inter-related boiling and condensation processes.

However, although smaller filling ratios (typically around 30 %) seem to correspond to better performance, they also mean less available surface for heat source location; a compromise has then to be reached between heat transfer capability and degree of freedom on heat source positioning.

Influence of inclination

The effect of the spreader inclination is also investigated. The experimental set-up is built to investigate inclination angle θ between 0° (with evaporator on top) and 180° (evaporator on the bottom), 90° corresponding to the vertical usual operating configuration for a two-phase thermosyphon. The 0° position is expected to be the most unfavorable one, with the evaporator wall not being in contact with the liquid pool; classical TPCTs do not operate in horizontal position and rarely exhibit good thermal performance when strongly inclined in general.

Despite the large range of inclination angles that was tested for various heating and cooling conditions, the effect of inclination on thermal resistance is hardly noticeable, as presented in Figure 10a for three different filling ratios in Config 2. Indeed, the uncertainty in the spreader thermal resistance does not allow to conclude on the very small differences induced by inclination changing. In limit cases (for example at very low filling ratio plus high heat flux), changes in the flow pattern were observed with nucleation reduction when inclining the spreader from 90° to 180° but they rarely led to an important degradation of thermal performance. Even in the least favorable horizontal position, no operation interruption occurred, which confirms that the gravitational forces are not dominant in the force balance. A maximal increase of 17 % in the thermal resistance was measured in the worst positions tested (horizontal with evaporator on top, at low filling ratios) compared to the vertical configuration for standard operation, which is not even significant if the uncertainty in the resistance is taken into account.

This low sensitivity to inclination can be explained by the system confinement that causes the internal wall on the evaporator side to be still correctly wetted by the liquid on a sufficient portion of its height even in the worst configurations, unlike in the case of classical thermosyphons. This is illustrated in Figure 10b (plotted for an inlet cooling temperature of 20°C to better highlight the different trends, in Config 2) by the relative uniformity of the maximal temperature at the evaporator $T_{wall,max}$ that remains almost constant despite significant changes in θ, whereas the influence of the inclination can clearly be seen on the wall temperature measurement just above the evaporator section, depending on which height is rewetted by the liquid in the inclined spreader.

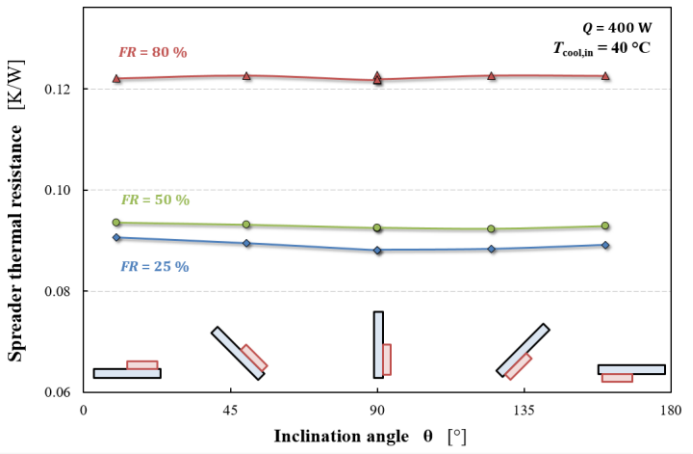

(*a*) spreader thermal resistance according to the inclination angle for various filling ratios [Config 2].

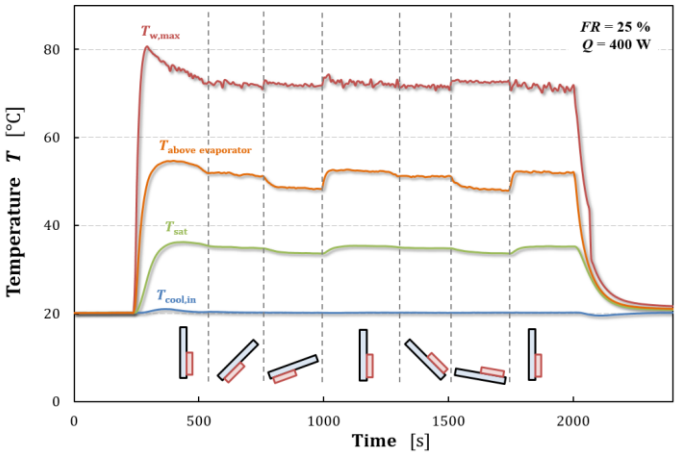

(*b*) example of temperature evolutions with changes in the inclination angle [Config 2].

Figure 10. Influence of inclination on the heat spreader thermal performance.
(bottom: corresponding positions of heat spreader and heat source)

These results are quite different from what is usually found in the literature for classical TPCTs. As previously mentioned, the few studies that investigate the effect of inclination angle (Noie *et al*, 2007; Hu *et al*, 2016; Li and Lv, 2016…) all conclude that this parameter has an important influence on the thermal performance and highlight the existence of an optimum position between vertical position and horizontal position with evaporator on the bottom. In the present work, the confinement allows to free the spreader from issues related to changes in inclination.

Influence of saturation temperature

The effect of the saturation temperature on flow patterns has already been mentioned in the section about flow visualizations: its influence on boiling processes and nucleation is clearly visible and changes in this operating parameter are therefore expected to significantly play in the thermal performance. Unfortunately, precise measurements of the saturation temperature are difficult to perform and its impact on the thermal resistance is often assessed through simple adjustments of the cooling temperature in the condenser region. In the present work, the saturation temperature is estimated with an average value of two vapor temperature measurements provided by thermocouples inside the cavity, and varied by setting different values of inlet cooling temperature $T_{cool,in}$.

Figure 11 presents the evolution of the spreader thermal resistance according to the saturation temperature for four filling ratios. The measurement points around each vertical grey line were obtained by setting the inlet cooling water temperature at the value written beneath it. As can be seen, the thermal resistance decreases with increasing saturation temperature until dry-out and the evolution is almost linear, with similar slopes for all filling ratios. Although increasing the saturation temperature leads to better performance in terms of thermal resistance, it also causes a global increase in the wall temperature, which might reach high values that are not suitable for the application, especially for the thermal management of electronic components. A compromise has then to be done depending on the specifications.

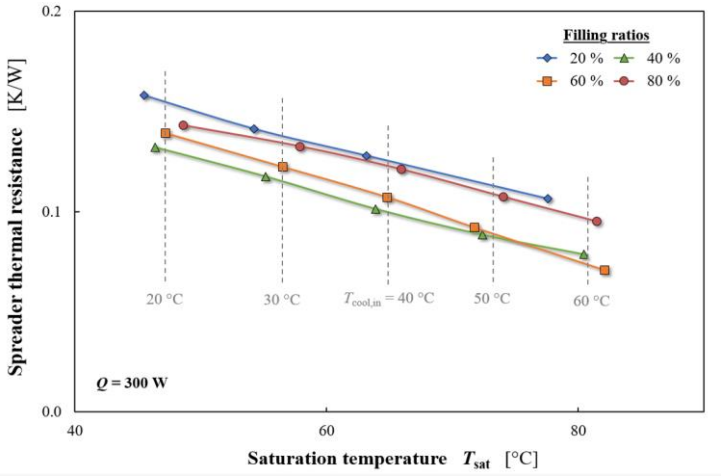

Figure 11. Evolution of the spreader thermal resistance with the saturation temperature for various filling ratios.

The evolution of the thermal performance with the saturation temperature can be correlated with flow visualizations: lower saturation temperatures (typically T_{sat} < 60 °C) correspond to flow regimes with nucleation of large bubbles at low frequency and therefore to limited heat transfer capability while higher saturation temperatures (T_{sat} > 60 °C) promote nucleation of small and dense bubbles enhancing heat transfers.

As explained, experimental studies on thermosyphons and flat heat pipes rarely investigate the influence of saturation temperature on thermal performance on extensive ranges; most of them often provide thermal resistance data for a given inlet cooling temperature only. Nevertheless, the few studies listed by Jafari *et al*. (2016) and Li and Lv (2016) which assessed the influence of cooling conditions on a thermosyphon or flat heat pipe thermal resistance found out similar trends with a degradation of the performance with a decrease of the saturation temperature.

3.3. Considerations of boiling and condensation coupling

Boiling and condensation mechanisms are affected by numerous operating parameters such as the saturation temperature or the filling ratio. Moreover, these two processes are strongly inter-related: because of the confinement of the heat spreader, they have significant influence over each other, as already observed by Zhang *et al* (2013), with the deviation of the tree bubbles on the sides due to the liquid return, for instance. Any slight modification in the device geometry or test conditions therefore causes significant changes in the flow pattern and / or thermal performance.

Figures 12 and 13 illustrate the effect of changes in the geometry or location of the heat source or heat sink. In Figure 12, the red dotted curve was obtained with the heat sink of Config 2 while the continuous blue one corresponds to Config 1 (meaning that only the position and dimensions of the heat sink vary between the two curves). Heating and cooling conditions, as well as filling ratio, were similar in the two experiments. Yet, the spreader thermal performance is clearly impacted by the heat sink repositioning, even when taking into account the uncertainty in the thermal resistance measurement. In this case, the cooling of the liquid pool by the large front heat sink may be the cause of the thermal degradation highlighted by the red curve. The differences induced by this type of changes (dimensions and location of heat sources) may be observed on the flow visualizations: in Figure 13, only the heat source dimensions are modified, as indicated in dotted lines: the top picture corresponds to Config 2 while the bottom one has been taken in Config 1. For a same heat flux, the difference in the thermal performance leads to differences in the nucleation regime, size and spread of the bubble tree and condensation process.

The coupling of boiling and condensation processes therefore makes the investigation of thermohydraulic behaviors even more complex. The characterization of thermal performance and flow patterns strongly depends on the chosen configuration (even the presence of the spacers plays a role), which complicates the correlation of flow visualizations (transparent heat spreader) with parametric runs (copper heat spreader).

For that reason, extensive characterization of the underlying thermohydraulic mechanisms has first to be performed with exhaustive flow patterns maps and large ranges of operating parameters in a single specific configuration; the investigation of the changes induced by modifications in the configuration (dimensions and position of heat source and / or heat sink) would then represent a further step towards the capability of designing devices for various applications.

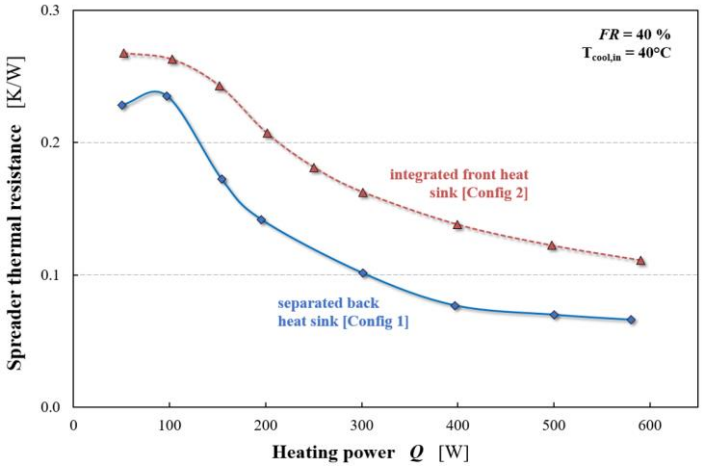

Figure 12. Spreader thermal resistance for heat sinks in Config 1 and Config 2 in the same operating conditions

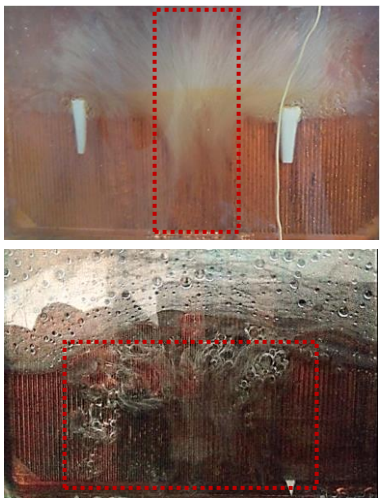

Figure 13. "Bubble tree" for heat sources in Config 2 (top) and Config 1 (bottom) in the same conditions

4. CONCLUSIONS AND PERSPECTIVES

Taking advantage of confined boiling phenomena in a flat thermosyphon allowed to build a novel two-phase heat spreader with interesting features for electronics cooling. Experiments including flow visualizations were performed to study both the underlying mechanisms and its thermal performance. They demonstrated that, despite complicated behavior characterization, this device can represent a viable solution for electronics cooling under challenging constraints such as in aeronautical applications. The flat confined thermosyphon exhibits:

- a suitable geometry for power modules and electronic components in addition to its compactness and simplicity;
- a high heat transfer capability (with a thermal resistance of 0.07 K/W for a 30 W/cm² heat flux at a 40 % filling ratio);
- a low sensitivity to changes in inclination with sufficient rewetted area in any configuration;
- a high degree of freedom for the heat sources location compared to a classical thermosyphon.

Further investigation for this study includes extensive characterization of flow patterns with the transparent spreader in various configurations in order to provide flow pattern maps, and additional experiments on thermal performance, at very high heat fluxes, for instance. Comparisons of thermal performance with equivalent conductive spreader and classical non-confined thermosyphons are also to be considered, as well as the assessment of the influence of additional parameters such as frozen start-up or working fluid, and more precise modelling / confrontation to models available in the literature.

5. ACKNOWLEDGEMENTS

This study was performed within the scope of the I²MPECT project with a funding of the European Commission N°H2020-MG-2014-636170.

6. REFERENCES

Bonjour, J., Lallemand, M., 1998. "Flow patterns during boiling in a narrow space between two vertical surfaces". *International Journal of Multiphase Flow*, Vol. 24, pp. 947-960.

Faghri, A., 2014. "Heat pipes: review, opportunities and challenges". *Frontiers in Heat Pipes 5*, pp. 1-48.

Franco, A., Filippeshi, S., 2013. "Experimental analysis of Closed Loop Two Phase Thermosyphon (CLTPT) for energy systems". *Experimental Thermal and Fluid Science*, Vol. 51, pp. 302-311.

Hu, M., Zheng, R., Pei, G., Wang, Y. Li, J., Ji, J., 2016. "Experimental study of the effect of inclination angle on the thermal performance of heat pipe photovoltaic/thermal (PV/T) systems with wickless heat pipe and wire-meshed heat pipe". *Applied Thermal Engineering*, Vol. 106, pp. 651-660.

Jafari, D., Franco, A., Filippeschi, S., Di Marco, P., 2016. "Two-phase closed thermosyphons: A review of studies and solar applications". *Renewable and Sustainable Energy Reviews*, Vol. 53, pp. 575-593.

Jouhara, H., Robinson, A.J., 2010. “Experimental investigation of small diameter two-phase closed thermosyphons charged with water, FC-84, FC-77 and FC-3283”. *Applied Thermal Engineering*, Vol. 30, pp. 201-211.

Li, J. and Lv, L., 2016. “Experimental studies on a novel thin flat heat pipe heat spreader”. *Applied Thermal Engineering*, Vol. 93, pp. 139-146.

Lips, S., Barrière, A., Narcy, M., Sartre, V., 2017. “Dispositif de diffusion thermique”. Patent FR 1750129.

Liu, S., Li, J., Chen, Q., 2007. “Visualization of flow pattern in thermosyphon by ECT”. *Flow Measurement and Instrumentation*, Vol. 18, pp. 216-222.

Noie, S.H., 2005. “Heat transfer characteristics of a two-phase closed thermosyphon”. *Applied Thermal Engineering*, Vol. 25, pp. 495-506.

Noie, S.H., Sarmasti Emami, M.R., Khoshnoodi, M., 2007. “Effect of inclination angle and filling ratio on thermal performance of a two-phase closed thermosyphon under normal operating conditions”. *Heat Transfer Engineering*, Vol. 28, No. 4, pp. 365-371.

Ong, K.S., Haider, M.D., Alalhi, E., 1999. “Experimental investigation on the hysteresis effect in vertical two-phase closed thermosyphons”. *Applied Thermal Engineering*, Vol. 19, pp. 399-408.

Ong, K.S., Tong, W.L., Gan, J.S., Hisham, N., 2014. “Axial temperature distribution and performance of R410a and water filled thermosyphon at various fill ratios and inclinations”. *Frontiers in Heat Pipe*, Vol. 5, No. 2.

Reay, D., McGlen, R., Kew, P., 2013. “Heat Pipes – Theory, Design and Applications”. 6th Edition, published by Butterworth-Heinemann.

Rops, C.M., Lindken, R., Velthuis, J.F.M., Westerweel, J., 2009. “Enhanced heat transfer in confined pool boiling”. *International Journal of Heat and Fluid Flow*, Vol. 30, pp. 751-760.

Smith, K., Byrne, G., Kempers, R., Robinson, A.J., 2016. “Electrohydrodynamic augmentation of a reflux thermosyphon”. *Experimental Thermal and Fluid Science*, Vol. 79, pp. 175-186.

Sobhan, C.B., Rag, R.L., Peterson, G.P., 2007. “A review and comparative study of the investigation on micro heat pipes”. *International Journal of Energy Research*, Vol. 31, No. 6-7, pp. 664-688.

Terdtoon, P., Waowaew, N., Tantakom, P., 1999. “Internal flow patterns of an inclined closed two-phase thermosyphon at critical state: case study II, effect of Bond number”, *Experimental Heat Transfer*, Vol. 12, pp. 359-373.

Tong, L., Chen, J., Cao, X., Yang, S., Liao, S., Deng, J., Zeng, W., 2015. “Visualization experiments on the geyser boiling-induced instability in vertical circular tube at low-pressures”. *Annals of Nuclear Energy*, Vol. 77, pp. 487-497.

Zhang, G., Liu, Z., Wang, C., 2013. “An experimental study of boiling and condensation co-existing phase change heat transfer in small confined space”. *International Journal of Heat and Mass Transfer*, Vol. 64, pp. 1082-1090.

Zhang, M., Lai, Y., Pei, W., Jin, L., 2014. “Effect of inclination angle on the heat transfer performance of a two-phase closed thermosyphon under low-temperature conditions”. *Journal of Cold Regions Engineering*, Vol. 28, No. 4.